ELSEVIER

International Journal of Heat and Fluid Flow 23 (2002) 792–806

International Journal of HEAT AND FLUID FLOW

www.elsevier.com/locate/ijhff

Thermo-mechanical modeling of turbulent heat transfer in gas–solid flows including particle collisions

Zohreh Mansoori [a], Majid Saffar-Avval [a], Hassan Basirat-Tabrizi [a], Goodarz Ahmadi [b,*], Santiago Lain [c]

[a] *Department of Mechanical Engineering, Amirkabir University of Technology, P.O. Box 15875-4413, Tehran, Iran*
[b] *Department of Mechanical and Aeronautical Engineering, Clarkson University, Box 5725, Potsdam, NY 13699-5725, USA*
[c] *Research Laboratory in Combustion Technology, LITEC/CSIC, Maria de Luna 10, 50015 Zaragoza, Spain*

Received 18 September 2001; accepted 13 March 2002

Abstract

A thermo-mechanical turbulence model is developed and used for predicting heat transfer in a gas–solid flow through a vertical pipe with constant wall heat flux. The new four-way interaction model makes use of the thermal k_θ–τ_θ equations, in addition to the hydrodynamic k–τ transport, and accounts for the particle–particle and particle–wall collisions through a Eulerian/Lagrangian formulation. The simulation results indicate that the level of thermal turbulence intensity and the heat transfer are strongly affected by the particle collisions. Inter-particle collisions attenuate the thermal turbulence intensity near the wall but somewhat amplify the temperature fluctuations in the pipe core region. The hydrodynamic-to-thermal times-scale ratio and the turbulent Prandtl number in the region near the wall increase due to the inter-particle collisions. The results also show that the use of a constant or the single-phase gas turbulent Prandtl number produces error in the thermal eddy diffusivity and thermal turbulent intensity fields. Simulation results also indicate that the inter-particle contact heat conduction during collision has no significant effect in the range of Reynolds number and particle diameter studied.

Keywords: Two-phase heat transfer; Gas–solid flow; k_θ–τ_θ Model and particle collisions

1. Introduction

Analysis of turbulent two-phase flows heat transfer, besides being of scientific interest, is of considerable practical importance in many industrial processes. For example, the rate of NO_x formation in a combustor with the same average temperature field depends on the temperature fluctuation. Dispersion of thermal pollutant in atmosphere, evaporation of spray droplets, and combustion of pulverized coal particles in boilers are examples illustrating the industrial importance of the thermal transport between the phases.

There are limited published works on temperature fluctuation field in multiphase turbulent flows. The thermal interactions between the phases are not as yet well understood. Jepson et al. (1963) reported the variation of heat transfer coefficient in a series of experimental studies. They showed that the suspension heat transfer coefficient has a U-shaped variation with solid loading ratio and is also affected by particle diameter. Soo (1967) formulated the statistical properties of the temperature fluctuations. Boothroyd and Haque (1970) reported the results of their experimental study on the heat transfer coefficient and friction factor in an upward fully developed pipe flow. They also found the U-shaped profile of heat transfer coefficient and friction factor versus solid loading ratios. Shraiber et al. (1990) showed heat the transfer from fluid to particles decreases as the size and heat capacity of particles increase. Using a two-fluid model with thermal eddy diffusivity concept, Han et al. (1991), studied heat transfer in a duct. They concluded that the decrease in the Nusselt number at low loading ratios is mainly due to the increase of the viscous sublayer thickness caused by the suppression of turbulence near the wall by the presence of solid particles. Using a Eulerian–Lagrangian model and

* Corresponding author. Tel.: +1-315-268-6536; fax: +1-315-268-6438.
E-mail address: ahmadi@clarkson.edu (G. Ahmadi).

0142-727X/02/$ - see front matter © 2002 Elsevier Science Inc. All rights reserved.
PII: S0142-727X(02)00187-X

Nomenclature

A	pipe cross-section, m^2
A_p	particle surface, m^2
A_l	lens area, m^2
c_p	specific heat, $J\,kg^{-1}\,°C^{-1}$
c_d	drag coefficient $= 24Re_p^{-1}(1 + Re_p^{0.667}/6)$
D	pipe diameter, m
d	particle diameter, m
e	restitution coefficient
$e_i(\mathbf{X}^+)$	shape factor
E	elastic modulus, Pa
F	$6Nu_pK_gd_p^{-2}$
F_L	Lift force, N
f	friction coefficient
f_μ	damping function $= (1 + 3.45Re_{t\theta}^{-1/2})\tanh(y^+/70)$
f_λ	damping function $= (1 + 2.4Re_{t\theta}^{-1/2})\tanh(y^+/120)$
f_l	drag factor
G	relative velocity vector
g_o	gravity acceleration, $m\,s^{-2}$
h_p	heat transfer coefficient, $W\,m^{-2}\,°C^{-1}$
$\mathbf{J}$	impulsive force, N
K	thermal capacity, $W\,m^{-1}\,°C^{-1}$
k	turbulent kinetic energy $= 1/2(\overline{u'_{gi}u'_{gi}})$, $m^2\,s^{-2}$
k_θ	temperature variance, $1/2\overline{t't'}$, $°C^2$
k_θ^+	non-dimension temperature variance $= k_\theta/T^{*2}$
K_g	gas heat conductivity, $W\,m^{-1}\,°C^{-1}$
l	effective distance (Fig. 1)
m	particle mass, kg
Nu	Nusselt number $= Dh_p/K_g$
p	pressure, $N\,m^{-2}$
Pr	Prandtl number $= \mu c_p/K_g$
Pr_t	turbulent Prandtl number $= \nu_t/\alpha_t$
q	heat flux, $W\,m^{-2}$
Q_p	heat transfer rate between particles, W
R_o	pipe radius, m
R	turbulent time scales ratio $= \tau/\tau_\theta$
r	radial coordinate
Re	Reynolds number $= DV\rho/\mu$
Re_T	turbulent Reynolds number $= k\tau/\nu$
$Re_{t\theta}$	thermal turbulent Reynolds number $= k\tau_\theta/\nu$
Re_p	particle Reynolds number $= \lvert u_i^g - u_i^p\rvert d_p/\nu$
Re_G	shear Reynolds number $= d_p^2/\nu(du/dy)$
S	source term due to solid phase
s	distance, m (Fig. 1)
T	mean temperature, °C
T_{gg}	gas temperature, °C
t'	temperature fluctuation, °C
T^*	friction temperature $= \alpha u^{*-1}(\partial T_g/\partial y)_{wall}$, °C
t	time, s
u	velocity, $m\,s^{-1}$
u'	velocity fluctuation, $m\,s^{-1}$
u^*	friction velocity $= [\nu(\partial U_g/\partial y)_{wall}]^{1/2}$, $m\,s^{-1}$
U	gas means velocity, $m\,s^{-1}$
v	particle velocity vector, $m\,s^{-1}$ (Fig. 1)
v_c	colliding particles relative velocity, $m\,s^{-1}$
x	vertical coordinates, m
y	distance from the wall, m
y^*	wall unit $= \nu/u^*$, m
y^+	non-dimension distance from the wall $= y/y^*$
z	loading ratio, solid mass flux/gas mass flux
X, Y, Z	coordinate system (Fig. 1)

Greeks

α	thermal diffusivity, $m^2\,s^{-1}$
α_t	thermal eddy diffusivity, $m^2\,s^{-1}$
β_1, β_2	contact angle
Δ	$\Delta = 3(1 - \sigma^2)/2E$
ε_X, ε_Z	directional cosine
ε	dissipation rate of turbulence kinetic energy, $\nu(\partial u'/\partial x_j)^2$, $m^2\,s^{-3}$
ε_θ	dissipation rate of turbulence thermal energy, $\alpha(\partial t'/\partial x_j)^2$, $°C^2\,s^{-1}$
ϕ	particle volume concentration
μ	viscosity, $kg\,m^{-1}\,s^{-1}$
ν	kinematic viscosity, $m^2\,s^{-1}$
ν_t	eddy viscosity, $m^2\,s^{-1}$
Θ	granular temperature, $3/2\Theta = 1/2\overline{v_p'^2}$, $m^2\,s^{-2}$
ρ	density, $kg\,m^{-3}$
σ	constant number
σ_s	Poisson ratio
τ	turbulence time scale, s
τ_θ	thermal turbulence time scale, s
τ_p	particle dynamic relaxation time, s

Subscripts and superscripts

c	contact
f	fluid
g	gas
gf	gas fluctuation
k	hydrodynamic intensity
L	Lift
n	normal component
o	pipe centerline
p	particle
t	tangential component
u	velocity
w	wall
θ	thermal turbulence
$'$	fluctuating part
$-$	average value
$+$	non-dimentional parameter
0	before collision

considering gas k–ε equations, Avila and Cervantes (1995) studied heat transfer coefficients in a pipe with constant wall temperature. Rizk et al. (1995) modeled the source term due to the solid phase in the fluid k_θ–ε_θ transport equations in a Eulerian approach in terms of particle relaxation time and turbulence time scale. Sato et al. (1998) studied the effect of fluid mean temperature gradient on heat transfer between dispersed and gas phases using a direct numerical method and an Eulerian–Lagrangian simulation. The one- and two-way coupling simulations of Jaberi (1998) showed that the thermal coupling is quite important. Andreux et al. (1999) used an Eulerian–Lagrangian model solving the momentum and energy equations for each phase.

Studies of the effect of inter-particle collision on the heat transfer in multiphase flows are rather scarce. Louge and Yusof (1993) used an Eulerian–Eulerian model and showed that particle collisions cannot be ignored even in dilute suspensions. While collisions are too rapid to permit direct heat transfer between particles and wall, they influence gas and particle temperature profiles and the rate of heat transfer. Berlemont et al. (1995) described different formulations for particle–particle collision in their hydrodynamic modeling approach. These are the Eulerian–Eulerian method, and the Eulerian–Lagrangian approach with direct simulation of particle–particle and particle wall collisions, and the Lagrangian approach with a stochastic collision model. The Eulerian–Eulerian approach was used by Simonin (1991) and Lavieville et al. (1995). They proposed a two-fluid model with the effect of inter-particle collision being incorporated through an analogy with the molecular dynamics. Hrenya and Sinclair (1997) developed a model that treated the individual particle interactions based on a kinetic theory and included the interactions associated with collection of particles based on an analogy with the single-phase turbulent flows. Using a four-way coupling, Berlemont et al. (1990) used the particle tracking approach including particle collisions. Tanaka and Tsuji (1991) also used a Eulerian–Lagrangian model including particle collisions for a vertical gas–solid pipe flow. Yonemura et al. (1993) performed a four-way coupled simulation accounting for non-elastic collisions. Stochastic collision model was developed by Sommerfeld and Zivkovic (1992) and Oesterle and Petitjean (1993). In this approach, the effect of collision is included stochastically through a local probability of collision model.

Sommerfeld (1995) showed that the particle collision has a significant effect on the particle velocity fluctuation field. In a subsequent study, Sommerfeld (1998) reported the effect of wall roughness on particle wall collision. Using a full Reynolds-stress model, Lain et al. (2001) conducted a four-way interaction modeling of gas–solid flows in a horizontal pipe. (Note that the four-way interaction modeling implies that the model accounts for inter-particle collisions in addition to the full interactions between the phases.) They presented experimental data for validating their numerical results. Using a one-way simulation and including the direct particle–particle collisions model, Mansoori et al. (2000) showed that the particle interactions and collisions could markedly influence the particle thermal fluctuation intensity.

The direct numerical simulation (DNS) of turbulent two-phase flows for homogeneous and isotropic turbulence was performed by Squires and Eaton (1990), and Elghobashi and Truesdell (1992). For two-phase turbulent flows in a channel, the DNS results were reported by Ounis et al. (1993) and Soltani and Ahmadi (1995). DNS methods, while exact, are limited to low Reynolds number flows. Therefore, the so-called large eddy simulation (LES) methods were developed to allow for handling of flows at higher Reynolds numbers. In LES filtered forms of the continuity and momentum equations are used to solve for the larger scales of turbulence and an eddy viscosity model is used for the unresolved smaller scales. Wang and Squires (1996) have applied the LES approach for analyzing the particle laden channel flows under the one-way interaction condition. Recently, Yamamoto et al. (2001) used an Eulerian–Lagrangian approach and studied the downward gas–solid flow in a vertical channel using LES to model the gas flow field. They also made a comparison of the flow fields with and without particle collisions.

The dynamic k–τ model was developed by Speziale et al. (1992) to overcome the lack of simple boundary condition for k–ε model. Schwab and Lakshminarayana (1995) showed that using the transport equations for dynamic and thermal turbulence time scales and kinetic energy, eliminates the difficulties of numerical problems in single-phase flows and leads to simpler wall boundary conditions. Saffar Avval et al. (2000) investigated the effect of thermal interaction between particles and turbulence temperature field in a vertical gas–solid pipe flow. They introduced the source term due to solid phase in the k_θ–τ_θ transport equations. The model showed that for a fully developed turbulent pipe flow, the solid phase causes thermal turbulent attenuation, and this effect is more significant for higher mass loading ratios and larger particle diameters. Using a one-way interaction simulation model, the effect of collision on the thermal turbulence attenuation was also studied by Mansoori et al. (2000). The model predicted that the collision causes the attenuation to be more important in the core region of the pipe. Recently, Mansoori et al. (2002) showed that the two-way interaction model is capable of determining the turbulent Prandtl number directly from the simulation. They, however, ignored the effect of particle collisions on heat transfer in their two-way interaction model.

In this study, a four-way interaction model for gas–solid flows using a Eulerian–Lagrangian approach is

described. In the earlier four-way interaction models, the inter-particle collisions were included, and the k–ε type formulation were used to account for the turbulence effects in both phases as well as heat transfer. The present model, however, makes use of the k_θ–τ_θ transport equations, in addition to a k–τ formulation for two-phase flows. Collisions between particles and between particle and the wall are also included in the analysis of the moment and thermal fields. That is, the interactions between the hydrodynamics turbulence and thermal turbulence including particle collision effects are accounted for the new formulation. The case of a fully developed turbulent two-phase flow in an upward pipe flow with constant wall heat flux is analyzed in details. A law of the wall boundary condition is used, and the simulation results are compared with the available experimental data and reasonable agreement is obtained.

2. Mathematical modeling

The formulation of a four-way interaction model for two-phase flows in a Eulerian–Lagrangian approach is described in this section. Assuming an incompressible and fully developed turbulent gas flow inside a vertical pipe, the mean velocity and temperature fields are evaluated by solving the time dependent Reynolds averaged conservation equations. The governing equations are closed with a k–τ model for the flow field and a k_θ–τ_θ model for the thermal field. The coupling source terms due to solid phase used in the k_θ–τ_θ equations are the extended form of those reported earlier by Saffar Avval et al. (2000) and Mansoori et al. (2002).

2.1. Hydrodynamic and thermal Analysis

The set of time-dependent closed equations for the mean gas velocity and temperature and the transport equations for k–τ and k_θ–τ_θ for a fully developed axisymmetric gas–solid flow in cylindrical coordinates is given as

$$\frac{D\left[(1-\phi)U_g\right]}{Dt} = \frac{1}{r}\frac{\partial}{\partial r}\left[r(\nu+\nu_t)(1-\phi)\frac{\partial U_g}{\partial r}\right] - (1-\phi)g_o - (1-\phi)/\rho_g\frac{\partial P}{\partial x} + S_u \quad (1)$$

$$\frac{D(1-\phi)k}{Dt} = \frac{1}{r}\frac{\partial}{\partial r}\left[r(1-\phi)\left(\nu+\frac{\nu_t}{\sigma_k}\right)\frac{\partial k}{\partial r}\right] + \nu_t(1-\phi)\left(\frac{\partial U_g}{\partial r}\right)^2 - (1-\phi)\varepsilon - S_k \quad (2)$$

$$\frac{D(1-\phi)\tau}{Dt} = \frac{1}{r}\frac{\partial}{\partial r}\left[r(1-\phi)\left(\nu+\frac{\nu_t}{\sigma_\tau}\right)\frac{\partial \tau}{\partial r}\right] + c_{\tau 1}(1-\phi) - c_{\tau 2}(1-\phi)\frac{\tau}{k}\nu_t\left(\frac{\partial U_g}{\partial r}\right)^2 + \frac{2}{k}(1-\phi)\left[\left(\nu+\frac{\nu_t}{\sigma_\tau}\right)\frac{\partial \tau}{\partial r}\frac{\partial k}{\partial r}\right] - \frac{2}{\tau}(1-\phi)\left[\left(\nu+\frac{\nu_t}{\sigma_\tau}\right)\frac{\partial \tau}{\partial r}\frac{\partial \tau}{\partial r}\right] + S_\tau \quad (3)$$

$$\frac{D(1-\phi)T_g}{Dt} = \frac{1}{r}\frac{\partial}{\partial r}\left[r(1-\phi)(\alpha+\alpha_t)\frac{\partial T_g}{\partial r}\right] + S_T \quad (4)$$

$$\frac{D(1-\phi)k_\theta}{Dt} = \frac{1}{r}\frac{\partial}{\partial r}\left[r(1-\phi)\left(\alpha+\frac{\alpha_t}{\sigma_{k\theta}}\right)\frac{\partial k_\theta}{\partial r}\right] + \alpha_t\left(\frac{\partial T_g}{\partial r}\right)^2 - \varepsilon_\theta - S_{k\theta} \quad (5)$$

$$\frac{D(1-\phi)\tau_\theta}{Dt} = \frac{1}{r}\frac{\partial}{\partial r}\left[r(1-\phi)\left(\alpha+\frac{\alpha_t}{\sigma_{\tau\theta}}\right)\frac{\partial \tau_\theta}{\partial r}\right] + c_{\tau\theta_1}(1-\phi)\frac{\tau_\theta}{k_\theta}\alpha_t\left(\frac{\partial T_g}{\partial r}\right)^2 + c_{\tau_\theta 2}(1-\phi) \times \frac{\tau_\theta}{k}\nu_t\left(\frac{\partial U_g}{\partial r}\right)^2 + (c_{\tau\theta 3}-1)(1-\phi) + \frac{2}{k_\theta}(1-\phi)\left[\left(\alpha+\frac{\alpha_t}{\sigma_{\tau\theta}}\right)\frac{\partial \tau_\theta}{\partial r}\frac{\partial k_\theta}{\partial r}\right] - \frac{2}{\tau_\theta}(1-\phi)\left[\left(\alpha+\frac{\alpha_t}{\sigma_{\tau\theta}}\right)\frac{\partial \tau_\theta}{\partial r}\frac{\partial \tau_\theta}{\partial r}\right] + c_{\tau\theta 4}(1-\phi)\frac{\tau_\theta}{\tau} + S_{\tau\theta} \quad (6)$$

Here ϕ is the solid volume fraction and $\nu_t = c_\mu f_\mu k\tau$ is the eddy viscosity, and $\alpha_t = c_\lambda f_\lambda k\tau_\theta$ is the thermal eddy diffusivity. The damping functionsf_μ and f_λ as introduced by Schwab and Lakshminarayana (1995) are listed in nomenclature. The source terms in Eqs. (1)–(6) due to the presence of solid phase are listed in Table 1.

Table 1
Source terms due to the presence of solid phase

Eq. (1)	$S_u = \frac{\rho_p}{\tau_p\rho_g}\left[\phi(U_p-U_g)\right]$, $\tau_p = \frac{4}{3}\frac{\rho_p d_p}{\rho_g C_D\lvert U_p-U_g\rvert}$
Eq. (2)	$S_k = -\frac{\rho_p}{2\rho_g\tau_p}\left[\overline{\phi}(\overline{u'_{pi}u'_{gi}} - \overline{u'_{gi}u'_{gi}}) + \overline{\phi' u'_{gi}}(U_p-U_g)\right] - \frac{\rho_p}{2\rho_g\tau_p}\left[\overline{\phi' u'_{gi}(u'_{pi}-u'_{gi})}\right]$
Eq. (3)	$S_\tau = \frac{S_k}{\varepsilon}(c_{\tau 3}-1)$
Eq. (4)	$S_T = \frac{F}{\rho_g c_{pg}}\left[\phi(T_p-T_g)\right]$, $F = 6Nu_p K_g/d_p^2$
Eq. (5)	$S_{k\theta} = -\frac{F}{2\rho_g c_{pg}}\left[\overline{\phi}(\overline{t'_p t'_g} - \overline{t'_g t'_g}) + \overline{\phi' t'_g}(T_p-T_g)\right] - \frac{F}{2\rho_g c_{pg}}\left[\overline{\phi' t'_g(t'_p-t'_g)}\right]$
Eq. (6)	$S_{\tau\theta} = \frac{S_{k\theta}}{\varepsilon_\theta}(c_{\tau\theta}-1)$

Table 2
Values of model coefficients

c_μ	c_λ	$c_{\tau 1}$	$c_{\tau 2}$	$c_{\tau\theta 1}$	$c_{\tau\theta 2}$	$c_{\tau\theta 3}$	$c_{\tau\theta 4}$	$c_{\tau\theta}$
0.09	0.2	0.92	0.44	0.27	−0.7	$[1-\exp(-y^+/4.8)]^2$	$(1.92-1)[1-\exp(-y^+/4.9)]^2$	2.0

In Table 1, u'_{gi} and u'_{pi} are, respectively, the fluctuation velocities of gas and particle phases, and ϕ' is the particle concentration fluctuation. In the subsequence analysis, the triple correlation terms in source terms are neglected. The gas–particle velocity correlation term $\overline{u'_{pi}u'_{gi}}$ is evaluated using a combined Eulerian–Lagrangian averaging procedure given as

$$\overline{u'_{pi}u'_{gi}} = \frac{1}{\Delta t_E N_p}\sum_{l=1}^{N_t}\sum_{n=1}^{N_p}\left[(u_{pi}-U_{pi})(u_{gi}-U_{gi})\right]\Delta t_L \tag{7}$$

where u_{pi} and u_{gi} are the instantaneous particle and gas velocities. Here, N_p is the number of particle in the computational cell, $\Delta t_E = N_t\,\Delta t_L$ and N_t is the number of Lagrangian time steps in each Eulerian time step. The summation over n (and division by N_P) indicates the ensemble averaging over the particles in each computational cell, and the summation over l (and division by N_t) denotes the temporal averaging over the Eulerian time step.

The generation of fluctuating components of fluid velocity in an isotropic turbulence with the use of a Continuous Gaussian Random Field (CGRF) model was suggested by Kraichnan (1970). This approach was extended to non-homogeneous flows by Li and Ahmadi (1993). Here the CGRF model is used to generate the instantaneous turbulence fluctuation of gas velocity and gas temperature.

The particle concentration-gas velocity correlation term is modeled using a gradient transport hypothesis. That is, $\overline{\phi' u'_{g1}} \approx \nu_t \sigma_{pg}^{-1}\partial\overline{\phi}/\partial r$, where σ_{pg} is taken to be a constant equal to 1. In Table 1, t'_g is the fluctuating gas temperature and t'_p is the fluctuating particle temperature. The correlation terms between particle concentration and gas temperature are modeled by a gradient transport hypothesis given as $\overline{\phi' t'_g} \approx \alpha_t \sigma_{tg}^{-1}\partial\overline{\phi}/\partial r$, where, $\sigma_{tg} = 1$ is a constant. The gas–particle temperature correlation term $\overline{t'_p t'_g}$ is evaluated using a combined Eulerian–Lagrangian averaging procedure similar to that used for the gas–particle velocity correlation in Eq. (7).

In Eqs. (1)–(6), the coefficients σ_k, σ_τ, $\sigma_{k\theta}$ and $\sigma_{\tau\theta}$ are chosen as 1, $c_{\tau 3}$ is assumed to be 2.0, and the rest of the coefficients are listed in Table 2.

2.2. Instantaneous turbulence fluctuation

According to Kraichnan (1970), the fluctuation component of the fluid velocity in an isotropic pseudo-turbulent field may be approximated by a continuous Gaussian random field given as

$$\mathbf{u}'^{+}_{gf}(\mathbf{X}^+,t^+) = \sqrt{\frac{2}{M}}\left\{\sum_n^M \mathbf{U_1}[\cos(\mathbf{K_n}\cdot\mathbf{X}^+ + \omega_n t^+)]\right\} + \sqrt{\frac{2}{M}}\left\{\sum_n^M \mathbf{U_2}[\sin(\mathbf{K_n}\cdot\mathbf{X}^+ + \omega_n t^+)]\right\} \tag{8}$$

where $\mathbf{X}^+$ is the position vector and all quantities are non-dimensionalized with the friction velocity u^* and kinematic viscosity.

$$u'^{+}_{gfi} = \frac{u'_{gfi}}{u^*}, \quad t^+ = \frac{tu^{*2}}{\nu}, \quad x_i^+ = \frac{x_i u^*}{\nu} \tag{9}$$

Here

$$\mathbf{U_1} = \varsigma_\mathbf{n}\times\mathbf{K_n}, \quad \mathbf{U_2} = \xi_\mathbf{n}\times\mathbf{K_n} \tag{10}$$

$$\mathbf{K_n}\cdot\mathbf{U_1} = \mathbf{K_n}\cdot\mathbf{U_2} = \mathbf{0} \tag{11}$$

The components of vectors $\varsigma_\mathbf{n}$, $\xi_\mathbf{n}$ and frequencies ω_n are picked independently from a Gaussian distribution with a standard deviation of unity. Each component of $\mathbf{K_n}$ is also a Gaussian random number with a standard deviation of 1/2. In Eq. (8) M is the number of terms in the series. Here $M = 100$ is used.

Eq. (8) generates an incompressible Gaussian random field, which is continuous in space and time and resembles an isotropic homogeneous turbulence. For application to non-homogeneous flows a scaling is used. That is, $u'^{+}_{gi} = u'^{+}_{gfi}(\mathbf{X}^+,t^+)e_i(\mathbf{X}^+)$, in which $e_i(\mathbf{X}^+)$ are the shape functions for the axial, vertical and transverse rms velocities (Li and Ahmadi, 1993).

Similar formulation may also be used for generating the instantaneous gas temperature fluctuations (Mansoori et al., 2002). That is, the non-dimensional fluctuation temperature $t'^{+}_g = t'_g/T^*$ is given as

$$t'^{+}_g(\mathbf{X}^+,t^+) = \sqrt{\frac{2}{M}}\left\{\sum_n^M T_1[\cos(\mathbf{K_n}\cdot\mathbf{X}^+ + \omega_n t^+)]\right\} + \sqrt{\frac{2}{M}}\left\{\sum_n^M T_2[\sin(\mathbf{K_n}\cdot\mathbf{X}^+ + \omega_n t^+)]\right\} \tag{12}$$

Here T^* is the local root-mean square gas temperature fluctuation. All random coefficients in Eq. (12) are generated similar to that of the Kraichnan model for the flow field, except for T_1 and T_2 that are picked from independent Gaussian distributions with a standard deviation of unity.

2.3. Particle Lagrangian simulation

The equation of motion for a spherical particle including the viscous drag and gravitational forces is given as

$$\frac{\mathrm{d}u_{\mathrm{p}i}}{\mathrm{d}t} = \frac{3c_{\mathrm{d}}\rho_{\mathrm{g}}}{4d_{\mathrm{p}}\rho_{\mathrm{p}}}\left|u_{\mathrm{g}i} - u_{\mathrm{p}i}\right|(u_{\mathrm{g}i} - u_{\mathrm{p}i}) + g_{\mathrm{o}} \tag{13}$$

$$\frac{\mathrm{d}x_{\mathrm{p}i}}{\mathrm{d}t} = u_{\mathrm{p}i} \tag{14}$$

Here $u_{\mathrm{p}i}$ is the particle velocity, $u_{\mathrm{g}i}$ is the instantaneous fluid velocity with $u_{\mathrm{g}i} = U_{\mathrm{g}i} + u'_{\mathrm{g}i}$, where $U_{\mathrm{g}i}$ is the fluid mean velocity, $u'_{\mathrm{g}i}$ is the fluctuating component and $c_{\mathrm{d}} = 24Re_{\mathrm{p}}^{-1}(1 + Re_{\mathrm{p}}^{0.667}/6)$ is the local drag coefficient.

In an earlier work, Cao et al. (1996) showed that the rotational energy of particles is less than 10% of their translational energy even for the case of dense granular flows. Therefore, for the present case of relatively low solid volume fractions, the effects of particle rotation and the Magnus lift force, which are expected to be small, are neglected.

The ratio of the Saffman (1968) lift force, $F_{\mathrm{L}} = 1.61\mu d_{\mathrm{p}}\left|u_{\mathrm{p}} - u_{\mathrm{g}}\right|Re_{\mathrm{G}}^{1/2}$, to the Drag force is given as

$$\frac{\text{Lift}}{\text{Drag}} = \frac{1.61(Re_{\mathrm{G}})^{1/2}}{(3\pi f_1)} \tag{15}$$

Here $Re_{\mathrm{G}} = (d_{\mathrm{p}}^2/v)(\mathrm{d}u/\mathrm{d}y)$ is the shear Reynolds number and $f_1 = (1 + Re_{\mathrm{p}}^{0.667}/6)$ is the correction to the drag coefficient. (The expression for the shear lift is valid as long as $Re_{\mathrm{G}} \ll 1$.) In this study, the shear lift force is comparatively small compared to the Drag force and is ignored in the particle dynamic equation given by (13).

When a particle strikes a wall, it is assumed that it will bounce from the surface. The rebound velocity of a solid particle from the wall is evaluated using the classical impulse equation for inelastic collisions. Here unless stated otherwise a coefficient of restitution of 0.85 is used.

Thermal energy equation of the particles is given as Crowe et al. (1998)

$$mc_p(\mathrm{d}T_{\mathrm{p}}/\mathrm{d}t) = h_{\mathrm{p}}A_{\mathrm{p}}(T_{\mathrm{gg}} - T_{\mathrm{p}}) + \dot{Q}_{\mathrm{p}} \tag{16}$$

where m is the particle mass, c_{p} is the particle heat capacity, A_{p} is the particle surface area and h_{p} is the heat transfer coefficient. Here T_{p} is the particle temperature, and T_{gg} is the fluid temperature at the particle location. Note that $T_{\mathrm{gg}} = T_{\mathrm{g}} + t'_{\mathrm{g}}$, where t'_{g} is the gas fluctuating temperature, which is generated using the extended Kraichnan (1970) model. The heat source term, $\dot{Q}_{\mathrm{p}} = \dot{Q}_{\mathrm{pp}} + \dot{Q}_{\mathrm{pw}}$, is due to the heat transfer rate between adjacent particles $\dot{Q}_{\mathrm{pp}}$, and particles–wall heat transfer rate $\dot{Q}_{\mathrm{pw}}$. The procedure for evaluating magnitude of the heat source terms will be described in the subsequent section.

The convection transfer coefficient h_{p} is evaluated from the expression given in Crowe et al. (1998). That is

$$Nu_{\mathrm{p}} = h_{\mathrm{p}}d_{\mathrm{p}}/K_{\mathrm{g}} = 2 + 0.6Re_{\mathrm{p}}^{0.5}Pr^{0.3} \tag{17}$$

Here Nu_{p} is the particle Nusselt number K_{g} is the gas heat conductivity, and Pr is the Prandtl number.

2.4. Particle–particle and particle–wall collision model

Hard sphere particle–wall and particle–particle collisions are included in the present model. When considering mutual collisions between two particles, the decision on whether a particle collides with other particles is based on the centroid distance between the particles. Particle trajectories are obtained by integrating Eqs. (13) and (14) during in each Lagrangian time step.

The rebound velocities after inter-particle collisions are evaluated by the hard sphere model (Crowe et al., 1998). It is assumed that the particles will slide over one another during the collisions and the Coulomb friction law is used to relate the tangential and normal collision impulses. Inelasticity is considered in the context of the coefficient of restitution. The effect of particle rotation, which is expected to be small (Cao et al., 1996), is ignored. The particle deformation is also assumed to be negligible.

For the case of two identical particles, the linear impulse equations are given as

$$m_{\mathrm{p}}(\mathbf{v_1} - \mathbf{v_1^0}) = \mathbf{J} \tag{18}$$

$$m_{\mathrm{p}}(\mathbf{v_2} - \mathbf{v_2^0}) = -\mathbf{J} \tag{19}$$

where $\mathbf{v_1}$ and $\mathbf{v_2}$ are the velocities of particle 1 and 2 after collision and $\mathbf{v_1^0}$ and $\mathbf{v_2^0}$ are the velocities before collision, respectively as are shown in Fig. 1. Note that here the rotational motions are neglected. In Eqs. (18) and (19), $\mathbf{J}$ is the collision impulse force vector that may be divided into the normal and tangential components as $\mathbf{J} = J_{\mathrm{n}}\mathbf{n} + J_{\mathrm{t}}\mathbf{t}$, where $\mathbf{n}$ and $\mathbf{t}$ are the normal and tangential unit vectors as shown in Fig. 1. Inelastic collisions are considered in the context of the coefficient of restitution, e. Assuming the particles slide over one another during the collision, the normal and tangential component impulsive force is given as

$$J_{\mathrm{n}} = -m_{\mathrm{p}}/2(1 + e)(\mathbf{n} \cdot \mathbf{G^0}) \tag{20}$$

$$J_{\mathrm{t}} = fJ_{\mathrm{n}} \tag{21}$$

where $\mathbf{G^0} = \mathbf{v_1^0} - \mathbf{v_2^0}$ is the relative velocity between center of particles before collision and f is the friction coefficient. Thus, the post-collision velocities for the sliding collision are obtained as

$$\mathbf{v_1} = \mathbf{v_1^0} - 1/2(1 + e)(\mathbf{n} \cdot \mathbf{G^0})(\mathbf{n} - f\mathbf{t}) \tag{22}$$

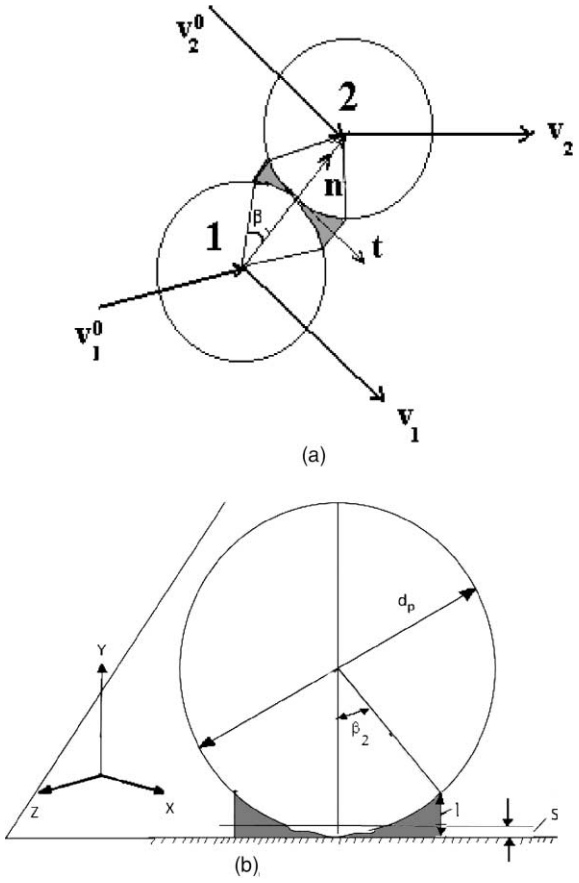

Fig. 1. (a) Schematics of particle–particle collisions and the corresponding pre and post collision velocities. (b) Schematics of particle–wall collisions and the wall coordinate system (X, Z). Shadow regions are the gas lens between wall and particle.

$$\mathbf{v}_2 = \mathbf{v}_2^{\mathbf{0}} + 1/2(1+e)\left(\mathbf{n}\cdot\mathbf{G}^{\mathbf{0}}\right)(\mathbf{n} - f\mathbf{t}) \tag{23}$$

The post-collision relative velocity $\mathbf{G} = \mathbf{v_1} - \mathbf{v_2}$ is related to pre-collision velocity through the restitution coefficient. i.e.,

$$\mathbf{n}\cdot\mathbf{G} = -e\left(\mathbf{n}\cdot\mathbf{G}^{\mathbf{0}}\right) \tag{24}$$

The wall bouncing process is influenced by the impact angle and particle velocity and particle and wall material parameters. Sommerfeld (1998) showed that wall roughness significantly affects the average rebound angle. For polished walls, he found that the rebound angle is nearly equal to the impact angle, for impact angles $< 10°$.

In the present study, the hard sphere model of wall–particle interaction described in Crowe et al. (1998) is used. For small friction coefficient, it is assumed that the condition: $-2/[7f(e_w+1)] \leqslant v_Y^0/|\mathbf{v}^{\mathbf{0}}| < 0$ holds, thus the particles slide during the collision. Here $\mathbf{v}^{\mathbf{0}}$ is the approaching velocity vector and v_Y^0 is it velocity perpendicular to the wall. The explicit expressions for components of the rebound velocity in the presence of rebound and inelastic collisions in the coordinate system XYZ as shown in Fig. 1b are

$$V_X = V_X^0 + \varepsilon_X f(1+e_w)V_Y^0 \tag{25}$$

$$V_Y = -e_w V_Y^0 \tag{26}$$

$$V_Z = V_Z^0 + \varepsilon_Z f(1+e_w)V_Y^0 \tag{27}$$

Here ε_X, ε_Z are direction cosines of approach velocity in the X–Z plane and e_w is restitution coefficient of wall–particle collision. In the present study, the particle rotation and the wall roughness effects are the neglected, and the wall–particle friction factor is also assumed to be negligible.

During particle–particle and particle–wall collisions, heat transfer could occur by radiation, conduction at the contact point, and conduction through the gas lens near the contact point. The radiation heat transfer, which is important at high temperatures, is negligible in this case. Louge and Yusof (1993) performed an order of magnitude analysis for the solid–solid conduction at the contact point for nearly elastic collisions. They estimated the ratio of equilibrium time of conduction through the adjacent solid particles to inter-particle collision time, which is given by

$$Rc \equiv \left(\rho_p^{1/5} d_p c_p\right) \Big/ \left(\Delta^{4/5}\Theta^{3/10}K_p\right) \tag{28}$$

where $\Delta = 3(1-\sigma^2)/2E$. Here, σ is the Poisson ratio and E is the elastic modulus, and Θ is the granular temperature (mean-square particle velocity fluctuations). For typical velocities common in gas–solid flows, they found that Rc is of the order of 10^6–10^8 and so the direct solid–solid conduction at the contact point is also comparatively small and can be neglected.

The heat transfer between particles by conduction through the gas lens, however, could become quite important and must be included in the analysis. Accordingly, when two particles with temperature T_i and T_j collide, the heat transfer through the gas layer at the contact point are given by (Delvosalle and Vanderschuren, 1985)

$$Q_{pp} = \Gamma(t_{cc})(T_{pi} - T_{pj}) \tag{29}$$

$$\Gamma(t_{cc}) = (1/2)K_g d_p \int_0^{\beta_1} (t_{cc}/\beta)\left\{\sin^2\beta/\left[2s/d_p + (1-|\cos\beta|)\right]\right\} d\beta \tag{30}$$

Here t_{cc} is the contact time, s is distance between two particle, and β_1 is the contact angle as shown in Fig. 1b. Experimental data of Delvosalle and Vanderschuren (1985) showed the contact angle β_1 is between 40°and 20°for particle diameters of 900–2250 μm. Extrapolating these data β_1 is assumed to be 50° for 500 μm particle.

Heat transfer through the gas lens between the wall and the particle was modeled by Molerus (1997). Accordingly, the particle–wall heat transfer is given as

$$Q_{pw} = h_w A_l (T_w - T_p) t_{cw} \tag{31}$$

where

$$Nu_w = h_w d_p / K_g = \pi\left[\left(1 + 2s/d_p\right) \times \ln(1 + d_p/2s) - 1\right] \tag{32}$$

Here t_{cw} is the particle–wall contact time during the collision, T_w is the wall temperature, and A_l is the lens area for contact heat transfer given by

$$A_l = \pi d_p l \tag{33}$$

$$l = d_p/2(1 - \cos\beta_2) + s \tag{34}$$

The distances s and l and the angle β_2 are shown in Fig. 1b. Note that s is the minimum distance between the particle and the wall (due to an effective roughness). For particles in air, s_{min} is 0.17 μm (Molerus, 1997). As noted before, the particle–wall contact angle, β_2 in Fig. 2b is chosen to be 50 °as β_1, and t_{cc} and t_{cw} are assumed to be equal to the contact time of as estimated by the Timoshenko and Goodier (1951) model, which is given as

$$t_c = 2.94\left(5/4\pi\rho_p 2^{1/2}\left(1 - \sigma^2\right)/E\right)^{2/5} d_p/2v_c^{-1/5} \tag{35}$$

Here, v_c is the collision velocity (which is the relative velocity of two colliding particles), σ is the Poisson ratio and E is the elastic modulus. Note that in Eq. (16), the heat transfers due to particle–particle and particle–wall collisions given by $Q_p = Q_{pp} + Q_{pw}$ where Eqs. (29) and (31) are used.

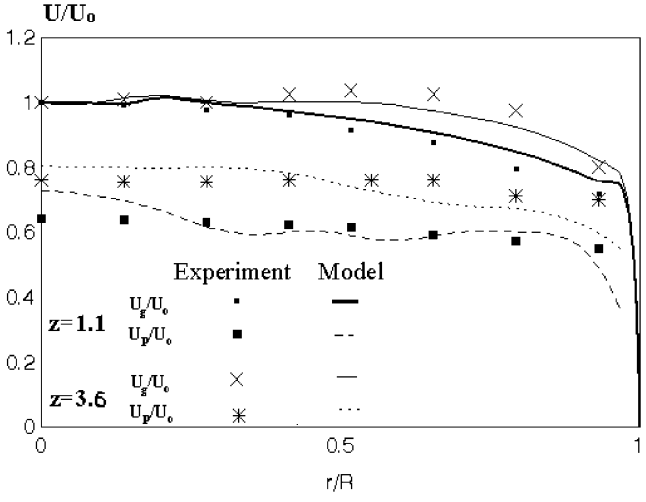

Fig. 2. Gas and particle velocity profiles at mass loading ratios of $z = 1.1$ and 3.6. Comparison with the experimental data of Tsuji et al. (1984) for $d_p = 500$ μm (solid lines: gas mean velocity; dashed and dotted lines: particle mean velocity; symbols: experimental results).

3. Numerical procedures

The time dependent computations are carried out for a turbulent axisymmetric quasi-fully-developed pipe flow with wall constant heat flux. An iterative procedure between Eulerian mean flow evaluation and the Lagrangian particle tracking is used to account for the four-way interactions as described in the following:

1. To start the solution procedure, the experimentally available data for fully developed single-phase gas flow is used as the initial gas flow condition. Using an interpolation scheme, the initial particle motion and temperature are evaluated.
2. The Lagrangian particle trajectory and heat transfer equations are solved in the known gas velocity and temperature fields, with particle–particle collisions being included. In this way the first estimate of individual particle locations, velocities and temperatures after each Lagrangian time step are evaluated.
3. At the next step the Eulerian field equations are modified by addition of the source terms due to presence of particles in the gas. Then the gas transport equations for U_g, T_g, k, τ, k_θ, τ_θ, including the solid-phase interaction source terms are solved.
4. After obtaining the converged solution for gas phase mean velocity and temperature and turbulence mechanical and thermal intensities, as well as time scales, all particles are tracked again in order to evaluate their corrected positions and an improved new interaction source terms.
5. Following Lain et al. (1999), the Lagrangian time step is chosen to be smaller than 10% of the following time scales:
   - the time required for a particle to cross the control volume,
   - the particle response time,
   - the local time scale of turbulence.
6. This iterative procedure is repeated until the convergence is achieved.

Wall boundary conditions are assumed as:

$$U_g = k = k_\theta = \tau = \tau_\theta = 0 \qquad K_g \partial T_g/\partial r = q_w \tag{36}$$

At the centerline the symmetric conditions for all variables are imposed.

Similar to the model of Andreux et al. (1999) and Louge and Yusof (1993) model, the governing equations for U_g, k, τ, k_θ, τ_θ are solved in the core region (between the pipe center and a node located at $y^+ = 30$), while the gas mean temperature equation is solved in entire region (up to the wall). Therefore, the computational boundary condition at the first grid next to the wall for U_g, k, τ, k_θ, τ_θ are given as $\partial k/\partial r = \partial k_\theta/\partial r = \partial\tau/\partial r = \partial\tau_\theta/\partial r = 0.0$. The law of the wall for the velocity field is used.

$$\begin{aligned} y^+ \leqslant 5: &\quad U_g^+ = y^+ \\ 5y^+ \leqslant 30: &\quad U_g^+ = 5\ln y^+ - 3.05 \\ y^+ \geqslant 30: &\quad U_g^+ = 1/4\ln y^+ + 5.7 \end{aligned} \tag{37}$$

As noted before, to properly account for the heat transfer, the temperature equation was solved up to the wall, and the heat flux boundary condition given by Eq. (36) was used. The needed values of U_g, k, τ, k_θ, τ_θ for temperature calculation near the wall are obtained by an interpolation scheme between the wall values as given by Eq. (37) for velocity and the calculated values at the first grid from the wall (at about $y^+ = 30$). To increase the accuracy of temperature field close to the wall, the grid is chosen so that it is quite fine near the wall.

Linear interpolation scheme is used for evaluating τ and τ_θ between their predicted values at a certain distance from the wall (about $y^+ = 30$) and zero value at the wall. At the initial state, spherical glass particles are randomly distributed at the entrance region with an initial velocity equal to 80% of the gas mean velocity and initial mean temperature equal to 80% of the gas mean temperature. Due to non-uniform grid spacing, the number of particles in each element is chosen in such a way that the particle concentration would be uniform in pipe cross-section. For evaluating particle trajectories and temperatures, a periodic boundary condition is assumed. That is for each particle, which leaves the computational domain, another particle is assumed to enter from the opposite side with the same velocity and temperature. Particles are also assumed to bounce from the wall with a restitution coefficient of 0.85, and the wall is assumed to be polished and frictionless. For particle–particle collision, a restitution coefficient of 0.9 and a friction coefficient of 0.02 are used.

The inter-particle collision algorithm is based on the Lagrangian approach, where all particles are individually tracked and particles collisions are individually accounted for. In the computation, at first the velocity and position of particles are calculated without considering inter-particle collisions. Then the occurrence of collisions for all particles is examined. If the distances between particle centers on their track are less than the particle diameter, then collisions are assumed to occur. The impulse equations for the colliding particles along the line of Crowe et al. (1998) are solved and particle velocities after collision are evaluated.

When the particle is close to the wall (s_{min} is about 0.17 μm), the heat transfer through the gas lens between particle and wall is accounted for in the simulation. For this purpose the model described by Molerus (1997) is used. When the particle is sufficiently close to the wall, heat conduction through the gas lens between particle and wall is computed, ignoring the gas movement in the lens. The heat conduction through the solid material during the short contact time between the particle and the wall, which is negligibly small, is ignored.

4. Numerical validation

Since simultaneously measured data for flow and thermal conditions are not available, the model results are compared for with flow data and thermal fields, separately. Experimental data of Tsuji et al. (1984) were used to validate the hydrodynamic part of computational model, and the experimental data of Jepson et al. (1963) was selected comparison with the thermal part. Effects of particle collisions are further studied by comparing the Lagrangian part of the present model results for gas–solid flows in a horizontal channel with the one-way interaction simulations of Sommerfeld (1995).

The experimental data of Tsuji et al. (1984) for the mean gas and particle velocities for a mass-loading ratios z (solid mass flux/gas mass flux) of 1.1 and 3.6, and gas Reynolds number of about 16,000 in a vertical pipe of 30.5 mm inner diameter are reproduced in Fig. 2. In the experiment the gas centerline velocity was 9.65 m s^{-1} and the particles were polystyrene spheres with a density of 1020 kg m^{-3} and a diameter of 500 μm. The distance between the inlet and the test section was 5110 mm (with a length to diameter ratio of about 170); therefore, a fully developed flow condition at the section was prevailed. The model predictions for the conditions of Tsuji et al. (1984) are evaluated and the results are shown in Fig. 2 for comparison. This figure shows that the predicted mean gas and particle velocities are in good agreement with the experimental data.

Fig. 3 compares the ratio of the simulated axial gas root mean square (rms) velocity to pipe centerline velocity with the experimental data of Tsuji et al. (1984)

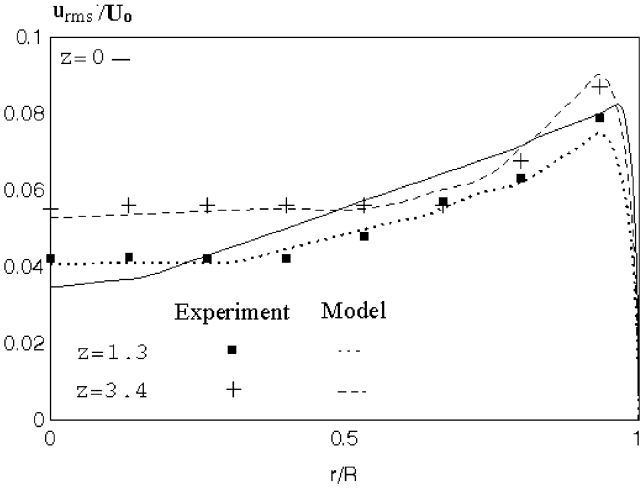

Fig. 3. Comparison of the results of the model for gas turbulence intensity with data of Tsuji et al. (1984) for $d_p = 500$ μm $z = 1.3$ and 3.4 (solid line: pure gas; dotted and dashed lines: present model; symbols: experimental results).

for mass loading ratios of 1.3 and 3.4 and $Re = 22{,}000$. Here, the gas centerline velocity is 13.4 m s^{-1}. Note that the computer simulation provides the value for the fluctuation kinetic energy. Using the anisotropy of fluctuation velocity from the experimental data for single-phase flow, the corresponding values of u_{rms} are estimated and are shown in Fig. 3. (That is, it is assumed that the values anisotropy of the fluctuation velocity remain roughly unchanged by the presence of particles for relatively dilute conditions.) It is seen that the turbulence intensity has a peak near the wall and decays toward the centerline. This figure also shows that the model predictions for the gas turbulence intensity are also in good agreement with the experimental data.

Fig. 4 compares the present model predictions for the suspension heat transfer coefficient, for various mass loading ratios with the experimental data of Jepson et al. (1963). The heat transfer coefficient is plotted versus the mass loading ratios. Here the pipe diameter is 0.038 m and constant wall heat flux is 630 W m^{-2}. The gas superficial velocities are 6, 12 m s^{-1} and the corresponding Reynolds numbers are about 11,000 and 22,000. The particles are sand with diameter of 500 μm. The Nusselt number is calculated using

$$Nu = 2R_o q_w / \left[K_g (T_w - T_m)\right] \tag{38}$$

where T_m is the mean suspension temperature, which is evaluated as

$$T_m = \left[\int c_{pg}\rho_g(1-\phi)U_g T_g \, dA + \int c_{pp}\rho_p \phi U_p T_p \, dA\right] \times \left[\int c_{pg}\rho_g(1-\phi)U_g \, dA + \int c_{pp}\rho_p \phi U_p \, dA\right]^{-1} \tag{39}$$

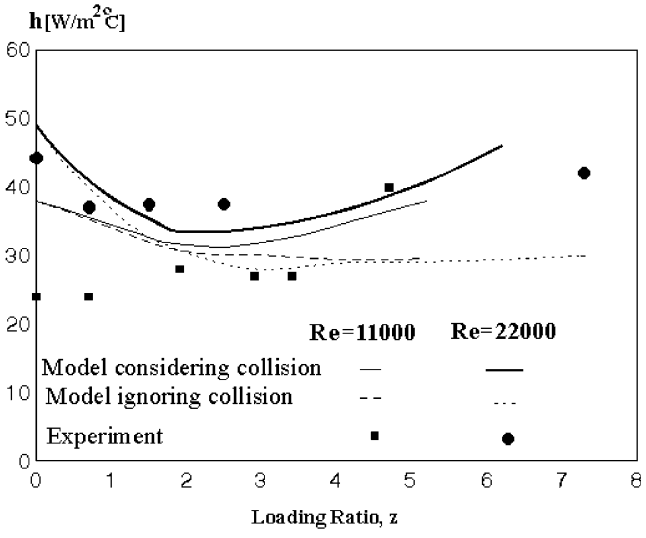

Fig. 4. Variation of suspension heat transfer coefficient versus mass loading ratio for $d_p = 500$ μm and different Reynolds numbers (solid lines: present model; dashed and dotted lines: model ignoring collision; symbols: experimental data of Jepson et al. (1963)).

The thermal conductivity of gas is computed at the film temperature $(T_m + T_w)/2$. The heat transfer coefficient for the single-phase gas flow is evaluated from the model at the limit of zero mass loading. The model prediction for the case that the inter-particle collisions are neglected is also shown in this figure for comparison.

When the inter-particle collisions are included, Fig. 4 shows that the model prediction is in reasonable agreement with the experimental data. It should be emphasized that the experimental data were obtained for the overall heat transfer coefficient, while the present numerical simulation assumed a fully developed condition. The model predictions show a U-shape variation of the heat transfer coefficient with the mass loading. For $Re = 22{,}000$, this figure shows a reasonable agreement between the model prediction and the experimental data. For $Re = 11{,}000$, data of Jepson et al. (1963) show a monotonic increase of the heat transfer coefficient with loading. The present model, however, predicts a U-shaped graph and thus over predicts the experimental results at low loading. The U-shape variation, however, is the expected trend and was observed in other cases (Boothroyd and Haque, 1970). Fig. 4 also indicates that the inter-particle collisions significantly affect the heat transfer coefficient especially at high loading. Ignoring collisions can cause the computed heat transfer to deviate from the experimental data at higher mass loading ratios.

Effects of particle collisions are further studied by comparing the present model results for gas–solid flows in a horizontal channel with the one-way interaction simulations of Sommerfeld (1995). In his paper, Sommerfeld modeled the inter-particle collision with a statistical method. In this case, the channel height is 30 mm and centerline gas velocity is 20 m s^{-1}. 100-micron particles with density of 2500 kg m^{-3} are dispersed randomly at the entrance region in a fully developed gas flow. For the conditions reported by Sommerfeld (1995), the present model is solved using a Cartesian coordinate system. With slight differences, the formulation in the Cartesian coordinate is similar to the axisymmetric one given by Eqs. (1)–(6). Fig. 5 compares the predicted normalized particle mass flux for different loading ratio with the simulation results of the statistical collision model of Sommerfeld (1995). It is seen that the particle mass increases toward the wall, and the particle collisions reduce the sharp increase of the mass flux near the wall. This figure also shows that the present model results are in good agreement with those of Sommerfeld (1995) for a low mass loading and when the collisional effects are neglected. At the mass loading of $z = 1$, there are some differences between the model predictions but the general trends are comparable.

In Fig. 6 a similar comparison is performed for the nondimensional root mean-square particle velocity fluctuations for different mass loading ratios of 0.1 and

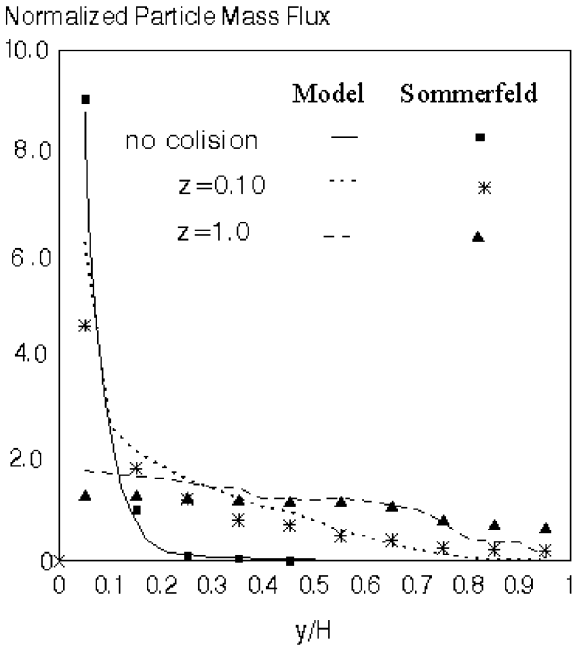

Fig. 5. Variation of particle mass flux normalized by the section averaged particle mass flux for different loading mass ratios in a horizontal turbulent channel (lines: present model; symbols: Sommerfeld (1995) results).

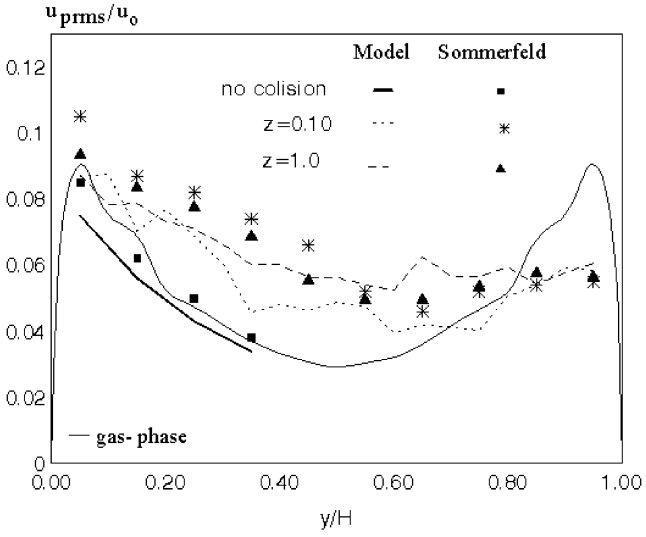

Fig. 6. Variation of horizontal component of mean particle fluctuation of velocity for different loading mass ratio in a horizontal turbulent channel (lines: present model; symbols: Sommerfeld (1995) results; thin solid line: gas single phase data).

1.0. The symbols in these figures are the results of the statistical collision model in the one-way interaction simulation reported in Sommerfeld (1995). Fig. 6 indicate that the predictions of the present model accounts directly for the inter-particle collisions for the particle root mean-square velocity are in general agreement with those of Sommerfeld's statistical model with the same mass loading ratios.

5. Results of parametric study

In this section the results of the parametric study of the new four-way interaction model are described. The importance of particle–particle collisions is first studied and the results are compared with the two-way simulations in the absence of inter-particle collision effects. This is followed by the study of the effect of inter-particle collisions on the gas and particle mean temperatures, root mean-square temperature fluctuations, turbulent Prandtl number and the time scale ratio, $R = \tau/\tau_\theta$. Parametric studies on variations of gas and particle mean temperatures and turbulence thermal intensity k_θ with mass loading ratio and particle diameter are also performed.

The experimental condition of Jepson et al. (1963) is used as the baseline for the numerical simulation studies. That is, unless stated otherwise, the gas superficial velocity is 6 m s^{-1} in a pipe with a diameter is 0.038 m. The wall heat flux is kept fixed at 630 W m^{-2}. The simulation was performed using a non-uniform mesh. A logarithmic scheme is used for the mesh generation. Typically a staggered grid of 30 is used. The maximum grid spacing of $\Delta y^+_{\max} = 101.0$ was at the pipe center and minimum spacing of $\Delta y^+_{\min} = 4.48$ was at the wall. Typically a Lagrangian time step of $\Delta t_L = 0.0001$ s is used. The Eulerian time step is about 10 times the Lagrangian one. In these simulations the number of particles used are 1000 for a mass loading of $z = 1$ that increases to 10,000 for $z = 4$. The typical flow parameters are listed in Table 3.

5.1. Inter-particle collision effect

The simulated gas and solid phase mean temperatures with and without the effect of inter-particle collisions are shown in Fig. 7. Here the mass-loading ratio is $z = 3$ and the solid is 500 μm sand particles. It is observed that the phasic mean temperatures have smooth variation decreasing from their peak near the wall toward the centerline. The particles are also somewhat cooler than the gas in the entire duct. Particle mean temperature also appears to be insensitive to inter-particle collision effect.

Table 3
Flow parameters used for parametric study

U_g (m s^{-1})	Re	u^* (m s^{-1})	y^* (mm)	t^* (ms)	ν (m^2 s^{-1})	α (m^2 s^{-1})	d_p (μm)	ρ_p (kg m^{-3})
6.0	11,000	0.375	0.053	0.124	2.103×10^{-5}	2.86×10^{-5}	500	1600

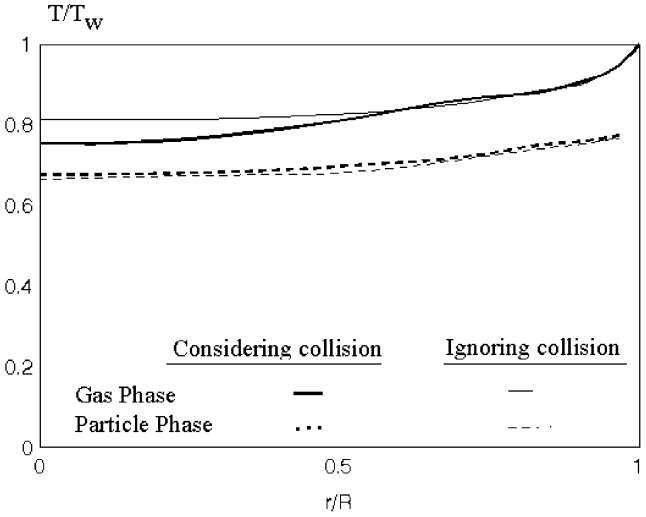

Fig. 7. Effect of inter-particle collisions on gas and solid phase mean temperatures for mass loading ratio of 3 and particles, $d_p = 500$ μm (thin lines: model-ignoring collision (two way); thick lines: model considering collision (four way); solid lines: gas phase; dashed lines: solid phase).

The gas mean temperature, however, is slightly less in the core region when the inter-particle collision effect is accounted for.

For different mass loading ratios, Fig. 8 compares the variation of the gas thermal turbulence intensity for the cases that the particle–particle collision effects are included in the analysis or ignored. In this figure k_θ^+ is gas temperature variance non-dimensioned by T^{*2}. The thick lines show the four-way interaction modeling (including the inter-particle collision effects), while the thin lines represent the two-way interaction results. It is observed that the thermal turbulence has a peak near the wall and decreases gradually towards the centerline. The presence of solids reduces the peak near the wall and increase k_θ^+ in the core regions. The attenuation of temperature fluctuation near the wall and its increase in the core region increases with the mass loading ratio and when the particle–particle collisions are accounted for. This observation indicates that the inter-particle collision amplifies the effect of solid phase and its importance increases at higher mass loading ratios.

Variations of turbulent Prandtl number Pr_t, (the ratio of kinematic eddy viscosity to thermal eddy diffusivity) across the pipe as a function of mass loading ratio are shown in Fig. 9. It is seen that the inter-particle collision effects significantly increase the turbulent Prandtl number near wall, while somewhat decrease it in the core region. That is, the inter-particle collision increases the ratio of the momentum transfer to thermal energy transfer in the near wall region. The effect also becomes more pronounced at higher mass loading ratios. Fig. 9 also indicates that use of single-phase gas turbulence Prandtl number and/or a constant Prandtl number that are commonly used may not be an acceptable approximation. In particular, neglecting the particle collision effect causes significant amount of error near the wall.

The ratio of mechanical time scale to thermal time scale $R = \tau/\tau_\theta$ is of considerable interest in single-phase flows. Warhaft and Lumley (1978) reviewed a number of single-phase turbulent gas flows with heat transfer. They also presented a set of experimental data for flows behind a grid and found that the ratio R is in the range of 0.6–2.4. The present model simulations with and without inter-particle collision effects are shown in Fig. 10.

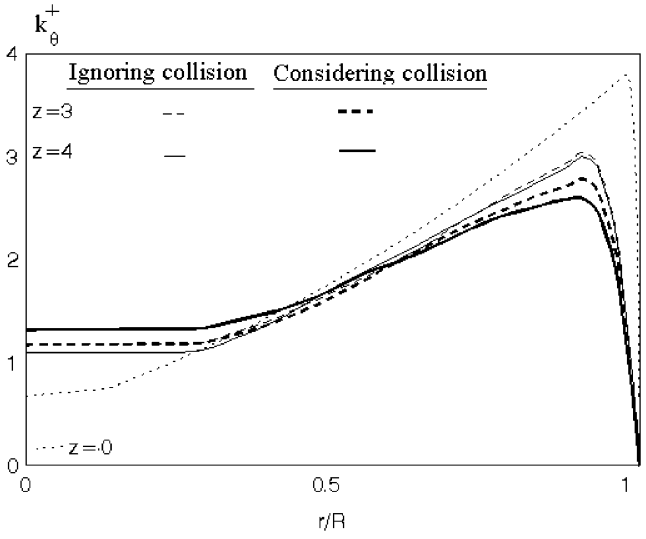

Fig. 8. Effect of inter-particle collisions on turbulence thermal intensity variation for different mass loading ratios for $d_p = 500$ μm (thin lines: model ignoring collision (two-way interaction); thick lines: model considering collision (four-way interaction); dotted line: $z = 0$).

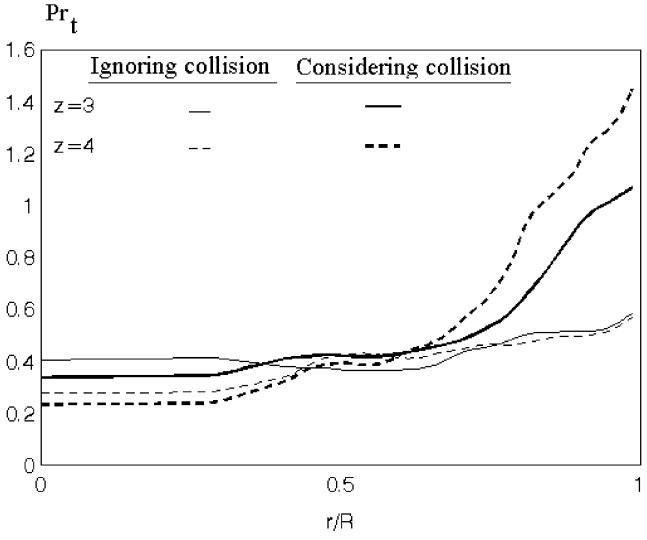

Fig. 9. Effect of inter-particle collisions on turbulence Prandtl number for mass loading ratios of 3 and 4 and particles with $d_p = 500$ μm (thin lines: model-ignoring collision (two-way interaction); thick lines: model considering collision (four-way interaction)).

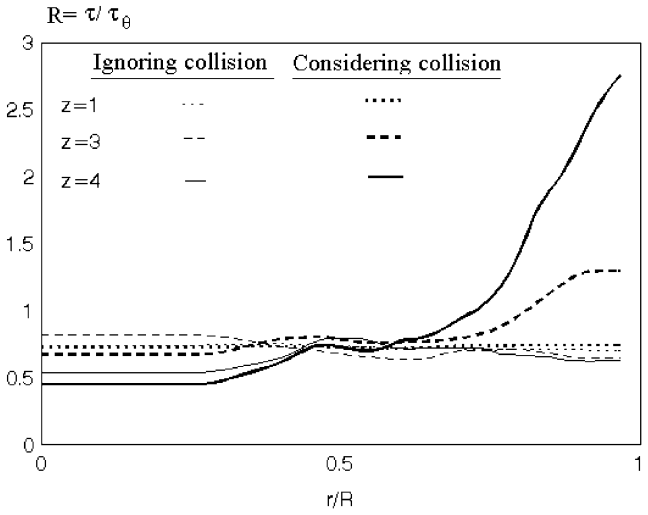

Fig. 10. Variation of $R = \tau/\tau_\theta$ for different mass loading ratios for $d_p = 500$ μm (thin lines: model ignoring collision (two-way interaction); thick lines: model considering collision (four-way interaction)).

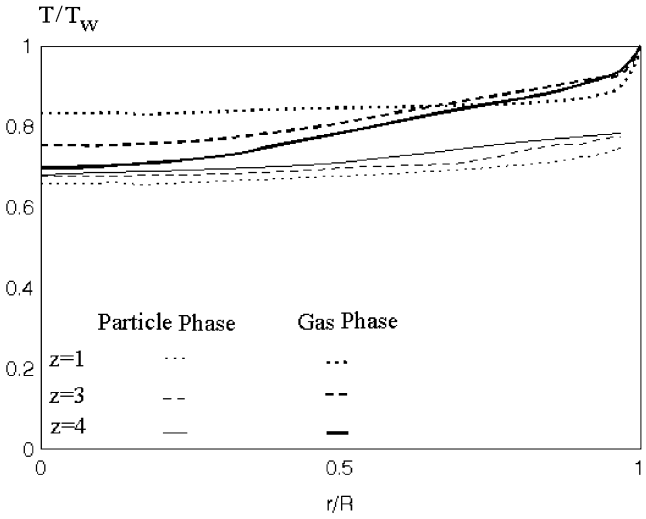

Fig. 11. Gas and solid phase mean temperatures for mass loading ratio of 1, 3 and 4 for particles with $d_p = 500$ μm (thick lines: gas phase; thin lines: particle phase).

When the effect of inter-particle collisions is included, it is seen that R is large near the wall and decreases toward the centerline. The variation of time scale ratio is completely distorted when the particle collisional effects are ignored. An increase in the mass-loading ratio also leads to a higher value of R in the near wall region. Fig. 10 clearly indicates that ignoring the inter-particle collision would cause considerable error in magnitude and trend of variation of R.

It is perhaps of interest to evaluate the order of magnitudes of the heat transfer between colliding particles, gas–particle and particle and wall. Eq. (16) may be restated as

$$mc_p\,\mathrm{d}T_p/\mathrm{d}t = \dot{Q}_{gp} + \dot{Q}_{pp} + \dot{Q}_{pw} \tag{40}$$

The numerical results shows that the ratio of inter-particle heat flux to the gas–particle heat transfer is of the order $\dot{Q}_{pp}/\dot{Q}_{gp} \cong \mathrm{O}(10^{-6})$ and the ratio of particle–wall heat flux to gas–particle heat transfer is of the order $\dot{Q}_{pw}/\dot{Q}_{gp} \cong \mathrm{O}(10^{-4})$.

These results show that the heat transfer effect during collision is generally small and the heat transfer is dominated by the particle–gas convection for the condition of the present study.

5.2. Effect of mass loading ratio and particle size

In this section the sensitively of model predictions to mass ratio and particle size are studied. Fig. 11 shows the variation of gas and solid mean temperatures for different mass loading ratios. Here the flow Reynolds number is 11,000, particles are sand with $d_p = 500$ μm, and all other conditions are identical to that of the experimental study of Jepson et al. (1963). Fig. 11 shows that the phasic mean temperature reduce gradually toward the core region with particle temperature being somewhat lower than the gas temperature. Furthermore, increasing the mass loading ratio causes the particle mean temperature to increase while it reduces the gas temperature. As a result, the phasic mean temperature difference decreases as z increases. This is due to the increase in the contact area of gas and solid that leads to improved heat transfer between two phases.

The corresponding variations of thermal turbulence intensity, k_θ^+ with mass loading across the pipe are shown in Fig. 12. It is seen that the root mean-square temperature fluctuation has noticeable peak near the wall and decreases toward the centerline. The presence

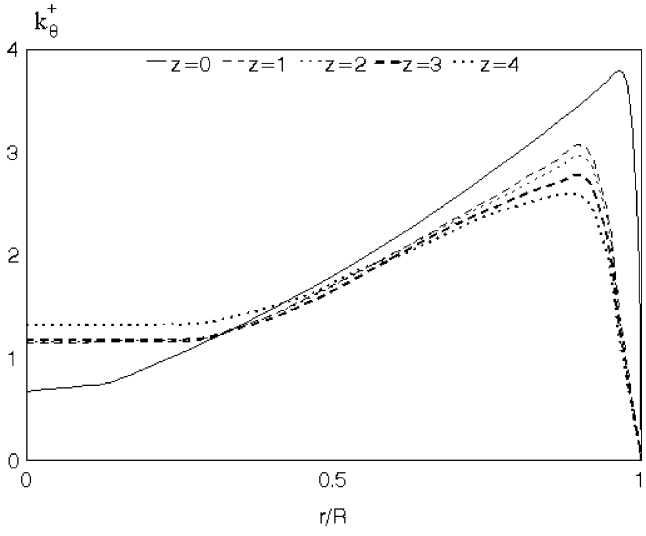

Fig. 12. Variation of turbulence thermal intensity for different mass loading ratios ($z = 0$, solid line; $z = 1$, dashed line; $z = 2$, dotted line; $z = 3$, heavy dashed line; $z = 4$, heavy dotted line).

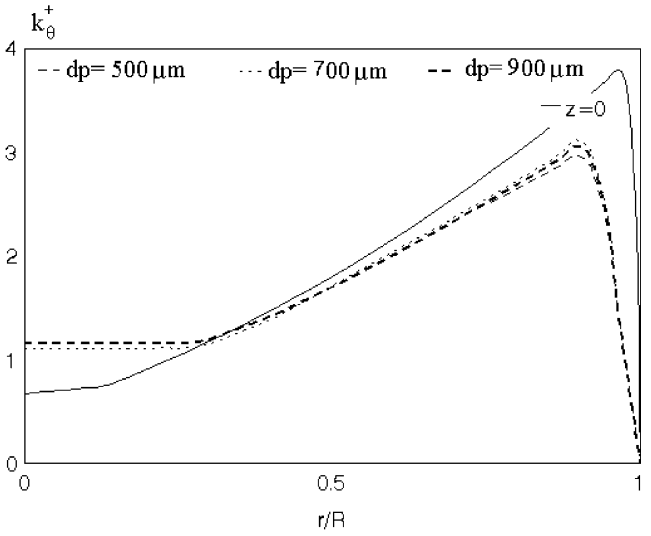

Fig. 13. Variation of turbulence thermal intensity for different particle diameters ($z = 0$, solid line; $d_p = 500$, dashed line; $d_p = 700$, dotted line; $d_p = 900$, heavy dashed line).

of particles attenuates the gas temperature fluctuations in the near wall region, and the amount of decrease increases with the mass-loading ratio. At a high mass loading of $z = 4$, presence of particles causes the gas temperature fluctuation in the core region to increase slightly.

For a mass-loading ratio of 2 and a flow Reynolds number of 11,000, variations of thermal turbulence intensity for different particle diameters are shown in Fig. 13. As noted before, the presence of particles attenuates gas temperature fluctuations near the wall, while increases it in the core region. Fig. 13 also shows that the effect of particles on k_θ increases slightly as particle diameter increases. Comparison of Figs. 12 and 13 indicates that the amount of attenuation near the wall is more sensitive to the variation of mass loading ratio than the particle diameter in the Reynolds number range studied.

6. Conclusion

Based on a new four-way interaction, two-phase flow and an Eulerian/Lagrangian formulation, a model for heat transfer in turbulent gas–solid flow is presented. The formulation includes the particle–particle collisions, in addition to the k–τ and the k_θ–τ_θ equations. The model was used to simulate upward vertical turbulent gas–solid flows in a fully developed pipe.

The presented thermo-mechanical results show that the root mean-square gas temperature fluctuation is generally attenuated by the presence of the particulate phase, while is increased in the core region of the pipe. The simulation results indicate that inter-particle collisions significantly affect the model predictions, especially at high mass loading ratios. This effect is due to changes in flow dynamic and inter-particle heat transfer has no significant effect in the range of Reynolds number and particle diameter studied. Inter-particle collision amplifies the effect of solid phase to decrease temperature intensity near the wall and increasing it in pipe centerline. Particle–particle collisions significantly affect the hydrodynamic to thermal times-scale ratio and also turbulent Prandtl number and cause those to be higher in the region near the wall. The presented results show that the use of single-phase gas turbulence Prandtl number and/or a constant turbulent Prandtl number is not an accurate assumption and causes error in calculating thermal eddy diffusivity and in consequence the thermal turbulent field. The results showed that the attenuation of gas temperature fluctuations near the wall is more sensitive to the variation of mass loading ratio when compared with to the particle diameter variation.

The presented model treats the variation of the coupled turbulent flow and thermal fields with no need for the Reynolds analogy assumption and/or a prescribed turbulence Prandtl number. The comparison of model prediction with experimental data shows reasonable agreement. However, further refinement of model in the near wall region is needed for improving the accuracy. Such refinement is currently under study.

Acknowledgements

The authors would like to acknowledge Professor Martin Sommerfeld of Martin-Luther University Halle/Saale (Germany) for his many helpful discussion on the modeling. Thanks are also given to Arash Shahrjerdi for his help in preparation of the figures. The work of GA was supported by the U.S. Department of Energy, National Energy Technology Laboratory (NETL).

References

Andreux, R., Boulet, P., Oesterle, B., 1999. Test of a Eulerian–Lagrangian simulation of wall heat transfer in a gas–solid pipe flow. In: Rodi, W., Laurence, (Eds.), Eng. Turbulence Modeling and Experiments-4. Elsevier Science, Amsterdam, pp. 913–922.

Avila, R., Cervantes, J., 1995. Analysis of the heat transfer coefficient in a turbulent particle pipe flow. Int. J. Heat Mass Transfer 38 (11), 1923–1932.

Berlemont, A., Desjonqueres, P., Gouesbet, G., 1990. Particle lagrangian simulation in turbulent flows. Int. J. Multiphase Flow 16, 19–34.

Berlemont, A., Simonin, O., Sommerfeld, M., 1995. Validation of inter-particle collision models based on large eddy simulation. ASME, FED, Gas–Particle Flows 228, 359–369.

Boothroyd, R.G., Haque, H., 1970. Fully developed heat transfer to a gaseous suspension of particles flowing turbulently in ducts of different size. J. Mech. Eng. Sci. 12 (3), 191–200.

Crowe, C., Sommerfeld, M., Tsuji, Y., 1998. Multiphase Flows with Droplets and Particles. CRC Press, Boca Raton, FL.

Delvosalle, C., Vanderschuren, J., 1985. Gas-to-particle and particle-to-particle heat transfer in fluidized beds of large particles. Chem. Eng. Sci 40 (5), 769–779.

Elghobashi, S., Truesdell, G.C., 1992. Direct simulation of particle dispersion in a decaying isotropic turbulence. J. Fluid Mech. 242, 655–700.

Cao, J., Ahmadi, G., Massoudi, M., 1996. Gravity granular flows of slightly frictional particles down an inclined bumpy chute. J. Fluid Mech. 316, 197–221.

Han, K.S., Sung, H.J., Chung, M.K., 1991. Analysis of heat transfer in a pipe carrying two-phase gas–particle suspension. Int. J. Heat Mass Transfer 34 (4), 69–78.

Hrenya, C.M., Sinclair, J.L., 1997. Effect of particle-phase turbulence in gas–solid flows. AIChE J. 43 (4), 853–869.

Jaberi, F.A., 1998. Temperature fluctuations in particle laden homogeneous turbulent flows. Int. J. Heat Mass Transfer 41, 4081–4093.

Jepson, G., Poll, A., Smith, W., 1963. Heat transfer from gas to wall in a gas/solid transport line. Trans. Instn. Chem. Eng. 41, 207–211.

Kraichnan, H., 1970. Diffusion by random velocity field. Phys. Fluids 11, 22–31.

Lain, S., Broder, D., Sommerfeld, M., 1999. Experimental and numerical studies of the hydrodynamics in a bubble column. Chem. Eng. Sci. 54, 4913–4920.

Lain, S., Kussin, J., Sommerfeld, M. 2001. Experimental studies and modeling of four-way coupling in particle-laden horizontal channel flow. Proc. 2nd Int. Symp Turbulent Shear Flow Phenomena, Stockholm, Sweden.

Lavieville, J., Deutsch, E., Simonin, O., 1995. Large eddy simulation of interactions between colliding particles and a homogeneous isotropic turbulence field. 6th Int. Symp. on Gas–Solid Flows, ASME, FED, vol. 228, pp. 347–357.

Li, A., Ahmadi, G., 1993. Computer simulation of deposition of aerosols in a turbulent channel flow with rough walls. Aerosol Sci. Technol. 18, 11–24.

Louge, M., Yusof, J.M., 1993. Heat transfer in the pneumatic transport of massive particles. Int. J. Heat Mass Transfer 36 (2), 265–275.

Mansoori, Z., Saffar Avval, M., Basirat-Tabrizi, H., 2000. The effect of particle particle interaction on heat transfer in a horizontal turbulent gas–solid channel flow. In: Loknath, M.S., Basu, B. (Eds.), 4th ISHMT/ASME Heat and Mass Transfer Conf., India, pp. 379–384.

Mansoori, Z., Saffar-Avval, M., Basirat Tabrizi, H., Ahmadi, G., 2002. Modeling of heat transfer in turbulent gas–solid flow. Int. J. Heat Mass Transfer 45, 1173–1184.

Molerus, O., 1997. Heat transfer in moving beds with a stagnant interstitial gas. Int. J. Heat Mass Transfer 17, 4151–4159.

Oesterle, B., Petitjean, A., 1993. Simulation of particle-to particle interactions in gas–solid flows. Int. J. Multiphase Flow 19, 199–211.

Ounis, H., Ahmadi, G., McLaughlin, J.B., 1993. Brownian particles deposition in a directly simulated turbulent channel flow. Phys. Fluids A 5, 1427–1432.

Rizk, M.A., Torki, A., El-Sallak, M., Mobarak, A., 1995. Mathematical modeling of heat transfer to gas–solid turbulent flows. ASME, FED, Gas–Particle Flows 228, 327–334.

Saffar Avval, M., Basirat Tabrizi, H., Mansoori, Z., 2000. The inter-particle effect on turbulent heat transfer in a gas–solid flow. In: Wolf, G.K. (Ed.), ASME/ ESDA Swiss. pp. 549–554.

Saffman, P.G., 1968. Corrigendum to the lift on a small sphere in a slow shear flow. J. Fluid Mach. 31, 624.

Sato, Y., Deutsch, E., Simonin, O., 1998. Direct numerical simulation of heat transfer by solid particles suspended in homogeneous isotropic turbulence. Int. J. Heat Fluid Flow 19, 187–192.

Schwab, J.R., Lakshminarayana, B., 1995. Dynamic and thermal turbulent time scale modeling for wall bounded shear flows. ASME, HTD, Heat Transfer Turbulent Flows 318, 111–118.

Shraiber, A.A., Gavin, L.B., Naumov, V.A., Yatsenko, V.P., 1990. Turbulent Flows in Gas Suspensions. Hemisphere, New York.

Simonin, O., 1991. Prediction of the dispersed phase turbulence in particle-laden jets. ASME, FED, Gas–Solid Flows 121, 197–206.

Soltani, M., Ahmadi, G., 1995. Direct numerical simulation of particle entrainment in turbulent channel flow. Phys. Fluid A 7, 647–657.

Sommerfeld, M., Zivkovic, G., 1992. Recent advances in the numerical simulation of pneumatic conveying through pipe systems. In: Hirsch, Ch., Periaux, J., Onate, E. (Eds.), Computational Methods in Applied Science, Brussels. pp. 201–212.

Sommerfeld, M., 1995. The importance of inter-particle collisions in horizontal gas solid channel flows. ASME FED Gas–Particle Flows 228, 335–345.

Sommerfeld, M., 1998. Modeling and numerical calculation of turbulent gas–solid flows with the Euler/Lagrange approach. Kona 16, 194–205.

Soo, S.L., 1967. Fluid Dynamics of Multiphase Systems. Blais-dell, Waltham, Massachusetts.

Speziale, C.G., Abid, R., Anderson, E.C., 1992. Critical evaluation of two-equation models for near wall turbulence. AIAA J. 30 (2), 324–331.

Squires, D.K., Eaton, J.K., 1990. Particle response and turbulence modification in isotropic turbulence. Phys. Fluids A 2, 1191–1203.

Tanaka, T., Tsuji, Y., 1991. Numerical simulation of gas–solid two-phase flow in a vertical pipe: on the effect of inter-particle collision. ASME, FED, Gas–Solid Flows 121, 123–128.

Timoshenko, Goodier, J.N., 1951. Theory of Elasticity. McGraw-Hill, NY.

Tsuji, Y., Morikawa, Y., Shiomi, H., 1984. LDV measurements of an air-solid two-phase flow in a vertical pipe. J. Fluid Mech. 139, 417–434.

Wang, Q., Squires, K.D., 1996. Large eddy simulation of particle-laden turbulent channel flow. Phys. Fluid 8, 1207–1223.

Warhaft, Z., Lumley, J.L., 1978. An experimental study of the decay of temperature fluctuations in grid generated turbulence. J. Fluid Mech. 88, 659–684.

Yamamoto, Y., Potthoff, M., Tanaka, T., Kajishima, T., Tsuji, Y., 2001. Large-eddy simulation of turbulent gas–particle flow in a vertical channel: effect of considering inter-particle collisions. J. Fluid Mech. 442, 303–334.

Yonemura, S., Tanaka, T., Tsuji, Y., 1993. Cluster formation in gas–solid flow predicted by DSMC method. ASME, FED, Gas–Particle Flows 166, 303–309.